CISK-Barotropic-Baroclinic Instability and the Growth of Monsoon Depressions

J. SHUKLA

Massachusetts Institute of Technology, Cambridge 02139

(Manuscript received 26 January 1977, in final form 14 November 1977)

ABSTRACT

A combined CISK-barotropic-baroclinic instability analysis of the observed monsoon flow has been performed using the quasi-equilibrium assumption for the parameterization of moist convection. Linear perturbation equations for a three-layer quasi-geostrophic model are numerically integrated to get the most unstable mode. A deep cloud model, in which the height of the base of the cloud does not change with time and entrainment occurs for the whole depth of the cloud but detrainment occurs only at the top, is used to parameterize the effects of moist convection.

It is found that the maximum growth rate occurs for the smallest scales. The mechanism for scale selection is therefore not clear. The structure and energetics of the computed linear perturbations for a wavelength corresponding to that of the observed monsoon depressions is compared with the observations. The dominant energy transformation for the computed and the observed perturbations is found to be from eddy available potential energy to eddy kinetic energy. The primary source of heating is condensational heating. Reasonable agreements between the structure and the energetics of the computed perturbations and the observed monsoon depressions suggest that CISK may provide the primary driving mechanism for the growth of monsoon depressions.

1. Introduction

Monsoon depressions, which form over the Bay of Bengal and move westward and west-northwestward and produce large amounts of rainfall over India, are among the most important components of the monsoon circulation. The horizontal scale of the depressions is about 2000–3000 km and the vertical scale about 10 km (Krishnamurti *et al.*, 1975). For the case studied by Krishnamurti *et al.*, the intense close vortex has a well-defined cold core in the lower troposphere and a warm core above 500 mb. The general direction of movement of these disturbances is between west and west-northwest (Fig. 1). Their phase speed is typically about 3 m s^{-1}. Due to scarcity of observations on the Burma coast, it is not possible to determine whether these disturbances formed over the Bay of Bengal or whether they originated further eastward. By examining the dates for which a cyclonic system was observed on the China coast, and the dates for which a monsoon depression appeared over the Bay of Bengal, Ramanna (1967) concluded that not more than 15% of the monsoon depressions would have developed from the westward moving perturbations which come from the China Sea. Similar conclusions were arrived at by this author after a subjective visual examination of the daily satellite cloud pictures for the months of June through September for the years 1967–73. It thus seems reasonable to assume that most of these disturbances develop over the Bay of Bengal and then move overland. The questions that are of primary interest are: What makes this area so cyclogenetic? Why do the monsoon depressions grow, or why do the weak perturbations which come from the east intensify after moving over this region?

Fig. 2a shows the cross section of mean monthly zonal wind speed for the month of July along 85°E from 20°S to 40°N. This cross section was prepared by combining the data presented by Koteswaram at the MONEX planning meeting at Singapore (1974, private communication) and the data interpolated from Ramage and Raman (1972). The vertical structure of the mean circulation is characterized by lower tropospheric westerlies, which attain a maximum speed of 40–60 kt at about 150 mb. The vertical shear is easterly (the meridional temperature gradient from south to north is negative), and the transition from lower level westerlies to upper level easterlies occurs at about 500 mb. The mean circulation is also characterized by appreciable horizontal shear. At 850 mb, the strongest westerlies occur at 10°N and are flanked by weaker easterlies in the foothills of the Himalayas and relatively stronger easterlies south of the equator.

Fig. 2b shows the vertical structure of temperature and moisture for the mean monsoon atmosphere. This vertical structure has been obtained from Saha and Singh (1972) and the India Meteorological Department

0022-4928/78/0495-0508$07.00

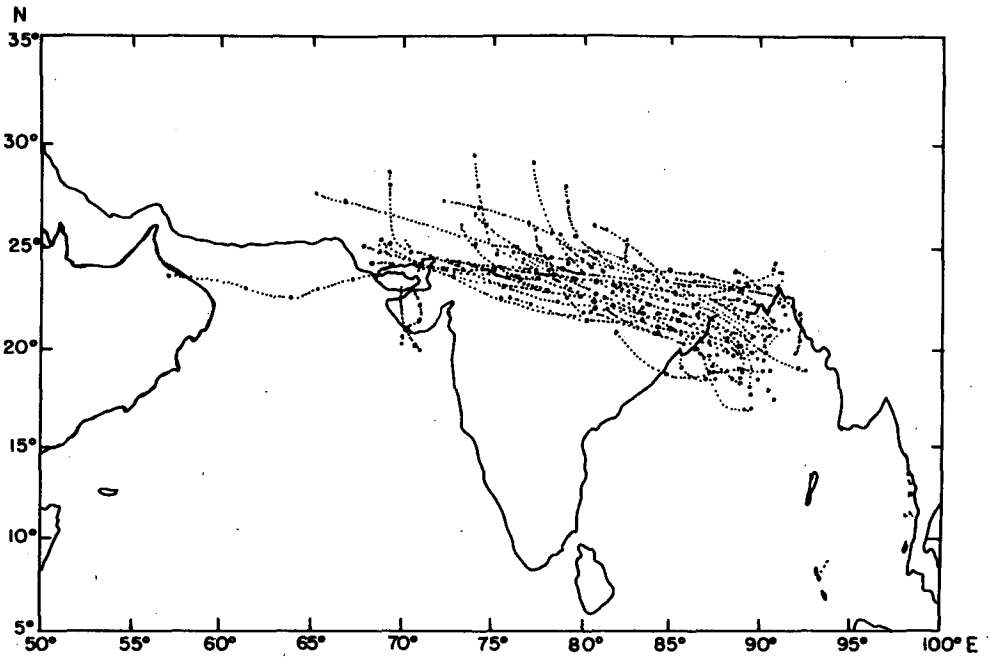

FIG. 1. Tracks of cyclonic storms during July for 1891–1960 (Indian Meteorological Department).

Forecasting Manual (1971). Moist static energy decreases from the surface value of 85.0 cal g^{-1} to 81.0 cal g^{-1} at about 3 km. Like the mean tropical atmosphere, the monsoon atmosphere is also conditionally unstable, with large values of mixing ratio in the lowest layers.

The purpose of this paper is to investigate the dynamics of these disturbances and to identify the physical mechanisms and dynamic instabilities which may be responsible for the growth and maintenance of these depressions. Since the mean monsoon state is characterized by horizontally and vertically shearing zonal winds, and since monsoon disturbances are accompanied by organized convective activity and precipitation, this work may also be viewed as a general study of the instability of a basic state in which the zonal wind has horizontal and vertical shear, the vertical thermal structure is conditionally unstable, and the moist con-

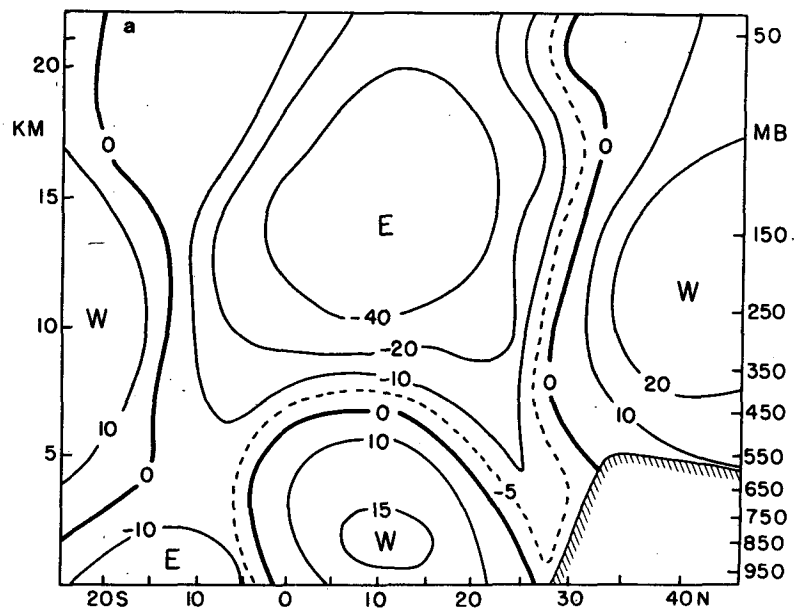

FIG. 2a. Cross section along 85°E for the observed mean July values of zonal wind.

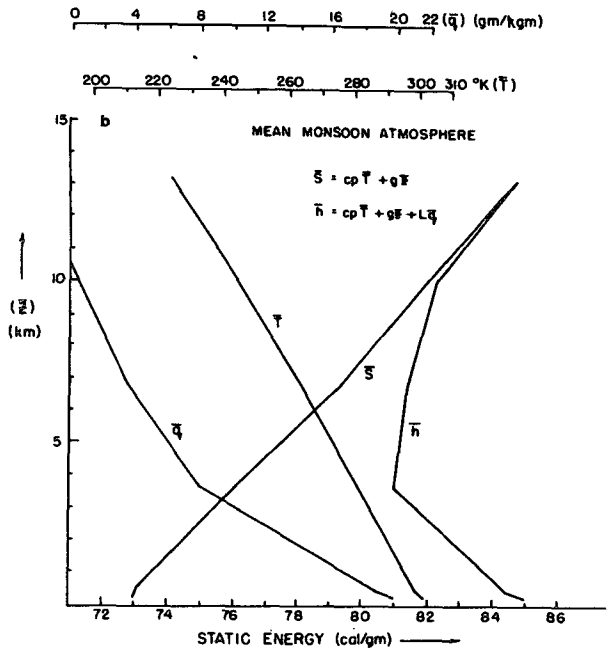

FIG. 2b. Vertical structure of temperature T, mixing ratio q, dry static energy S and moist static energy h for mean monsoon atmosphere.

vective heating is parameterized in terms of the large-scale variables. The basic approach here will be to investigate the role of CISK-barotropic-baroclinic instability mechanisms due to which infinitesimal perturbations upon the mean monsoon state may grow.

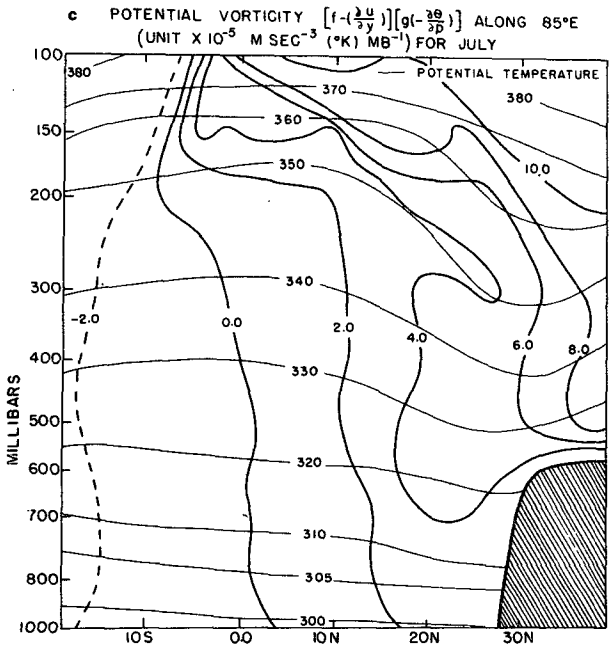

FIG. 2c. Cross section of potential vorticity [10^{-5} m s^{-3} mb^{-1} K] along 85°E.

a. The barotropic-baroclinic instability

One of the noteworthy features of the cross section of the zonal wind along 85°E (see Fig. 1) is the presence of a strong easterly wind between the two westerly maxima. Subtraction of a constant U (which is equivalent to a Galilean translation in the zonal direction) would readily show an internal jet. This suggests the possibility of an internal jet instability mechanism (Charney and Stern, 1962) in this region. One of the necessary conditions for this instability is that the gradient of potential vorticity on an isentropic surface should vanish in the region. A cross section of potential vorticity along 85°E (Fig. 2c) shows that this necessary condition for instability is satisfied. Krishnamurti *et al.* (1976) have shown that for the synoptic situation studied by them, the necessary condition for the Joint barotropic-baroclinic instability was satisfied; however, they did not perform the instability analysis.

Shukla (1977) examined the combined barotropic-baroclinic instability of mean monsoon zonal flow using a 10-layer quasi-geostrophic model. Because zonal current is a function of y and p, the problem becomes nonseparable (this is a manifestation of the fact that there are two sources of energy—available potential energy and available kinetic energy); therefore, the initial value approach to instability analysis was used. The preferred scale for the fastest growing mode was found to be ~3000 km. The structure and energetics of the most unstable mode were found to have no resemblance to the structure and energetics of the observed monsoon depressions. In particular, the amplitude of the barotropically unstable disturbance was maximum at 150 mb, whereas the observed monsoon depressions have their maximum amplitude at the lower level. It was therefore inferred that the barotropic-baroclinic instability alone may not be adequate to explain the formation and maintenance of monsoon depressions. In this paper we have included the effects of moist convective heating and investigated the joint CISK-barotropic-baroclinic instability.

b. The CISK

Charney and Eliassen (1964) have suggested that the development of tropical disturbances in a conditionally unstable atmosphere may be viewed as a kind of secondary instability in which the cumulus- and cyclone-scale motions cooperate, rather than compete, in such a way that the low-level synoptic convergence, as well as frictional convergence in the boundary layer, pumps moisture upward to the cloud base. The upward pumping is further accelerated by the latent heat of condensation. In response to the accelerating upward mass flux in the clouds, there is a compensating sinking in the immediate cloud environment. The associated heating by adiabatic compression increases the mean buoyancy and therefore the mean upward velocity

with height. The resulting stretching of the vortex tubes of the earth's vorticity intensifies the cyclonic vorticity and enhances the low-level convergence and therefore increases the heating. This mechanism is referred to as the Conditional Instability of the Second Kind (CISK) (Charney, 1973).

Although the CISK theory indicates that the moist-convective heating should be related to the total convergence of moisture into a vertical unit column, it does not determine how this heating should be distributed in the vertical. In the original formulations of Charney and Eliassen (1964) they took only two layers with equal heating and in Charney (1971) the thermodynamic equation was used only at one mid-atmospheric level where the heating was specified.

The determination of the actual vertical distribution of heating requires a parameterization of moist convection in a conditionally unstable atmosphere. In the past, several studies have been carried out with empirical or very simplified specifications of the vertical heating function.

In an earlier study, Shukla (1976) has examined the instability characteristics of a vertically sheared mean monsoonal flow, using empirical vertical distributions of CISK-type heating. In this formulation, heating was made proportional to the Ekman pumping, or to the vertical velocity at the top of the lowest layer. In either case, the wavelength of the fastest growing mode depended on the vertical distribution function for cumulus heating. Experiments were done with several vertical distribution functions. One of the noteworthy results was that the horizontal scale of the most unstable mode was larger for those heating profiles that provided heating to the larger vertical depths of the atmosphere. This result is consistent with the concept of the Rossby radius of deformation in the theory of geostrophic adjustment, in which the scales of the horizontal and the vertical circulations are interrelated through static stability and rotation. These calculations pointed out that one can simulate several kinds of tropospheric tropical disturbances by choosing suitable heating profiles. Since the choice of the heating profile is largely arbitrary, it points to the need of a theory for deducing the effects of the moist convection.

c. Quasi-equilibrium assumption (QEA)

Arakawa and Schubert (1974) have proposed the concept of quasi-equilibrium between the destabilizing large-scale forcing and the stabilizing effects of the cumulus ensemble. In this study, the quasi-equilibrium assumption (to be referred as QEA) has been applied to parameterize the effects of moist convection. It is recognized, as mentioned below, that this scheme involves some questionable assumptions concerning the interaction of the large-scale with the cumulus ensemble, and the structure and life cycle of the cumulus clouds.

SOME REMARKS ON THE ASSUMPTIONS AND LIMITATIONS OF QEA

1) It is assumed that the fractional cloud-covered area is very small. This assumption may not be valid for the eyewall region of a hurricane, and other active zones.

2) The cloud work function is determined only by the vertical thermal structure of the atmosphere. For phenomena such as squall lines and other types of rainbands, dynamical forcings are quite important. In such situations, the work function may have to be redefined.

3) It is assumed that the clouds are entraining through their whole vertical depth and detraining only at the level of vanishing buoyancy. This is not true for real clouds, because entrainment and detrainment both take place through the whole cloud depth simultaneously. This assumption may not be very serious if we only consider a spectrum of clouds because clouds of different size will have different levels of detrainment.

4) This parameterization scheme does not include the effects of evaporation of the rain falling from the convective clouds. The cooling due to the evaporation of the falling rain may be an important factor in determining the thermal structure of the tropical disturbances.

5) The observational evidence for the constancy of work function does not seem to be sufficient. More detailed data analysis for a larger variety of synoptic situations may be needed to establish the validity of this assumption. It is one of the unique characteristics of tropical disturbances that the temperature changes associated with them are quite small and, therefore, very careful analysis of accurate observations are needed to detect the small changes. Moreover, if constancy of the work function is a unique characteristic of the observed mean state, it is not clear if this scheme would be suitable for the simulation of a climate which has evolved from a different mean state.

6) The application of QEA turns out to be equivalent to some form of convective adjustment in which the computed cloud mass flux is the one which is needed to keep the atmosphere neutral.

7) The uniqueness of the solution of the integral equation involving the mass flux is not guaranteed. Different spectral distributions of the cloud mass flux may imply quite different vertical distributions for the heating.

8) A cloud type is characterized by only one parameter—its fractional rate of entrainment.

In spite of the several limitations, this scheme, for the first time, offers a rational closure hypothesis to determine the effects of a cumulus ensemble from the large scale variables; thus, the application of this scheme merits discussion.

Shukla (1976) studied the instability of a resting atmosphere with a three-layer quasi-geostrophic model

where cumulus heating was parameterized by QEA, and the lower boundary condition for vertical velocity was specified by Ekman pumping. It was found that the maximum growth rate occurred for a wavelength of intermediate scale, for which the vertically integrated net heating was also found to be maximum. This is in agreement with the results of Arakawa and Chao (1975, private communication).

It was also found for a resting atmosphere, if cumulus heating was parameterized by QEA, that there were no growing solutions in the absence of Ekman pumping or in the absence of Rayleigh friction in the lowest layer. If there is no surface friction, and if the disturbance is not propagating, it is not possible to generate internal vertical velocities in a resting atmosphere. Since heating is parameterized in terms of internal vertical velocity, heating is not realized in the absence of surface friction, and there are thus no growing modes. However, in the presence of surface friction, the frictional convergence associated with the infinitesimal perturbations produces Ekman pumping and internal vertical velocity. Since heating is parameterized in terms of internal vertical velocity, a perturbation may grow if the vertical structure of the internal vertical velocity of the perturbation is such that the application of QEA leads to a net heating of the atmosphere.

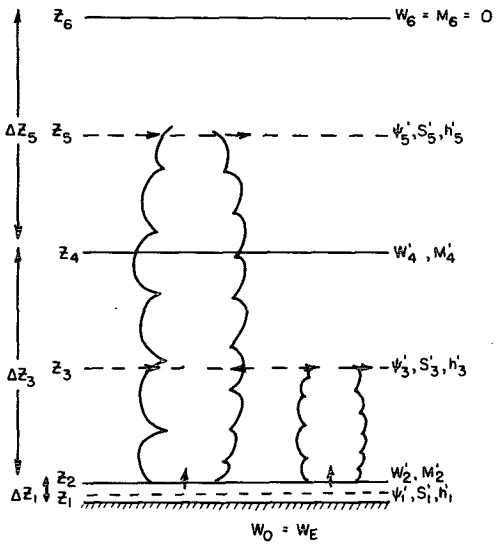

FIG. 3. Schematic representation of the three-layer model with shallow and deep clouds.

2. The mathematical model

The mathematical model used for this study is a three-layer quasi-geostrophic model. For the three-layer model shown in Fig. 3, the linearized perturbation equations are written in the following form:

$$\frac{\partial}{\partial t}\nabla^2\psi_1' = -\bar{U}_1\frac{\partial}{\partial x}\nabla^2\psi_1' - \frac{\partial\psi_1'}{\partial x}(\beta - \bar{U}_{1yy}) + \frac{f_0}{\rho_1\Delta Z_1}(W_2' - W_0') \tag{2.1}$$

$$\frac{\partial}{\partial t}\nabla^2\psi_3' = -\bar{U}_3\frac{\partial}{\partial x}\nabla^2\psi_3' - \frac{\partial\psi_3'}{\partial x}(\beta - \bar{U}_{3yy}) + \frac{f_0}{\rho_3\Delta Z_3}(W_4' - W_2') \tag{2.2}$$

$$\frac{\partial}{\partial t}\nabla^2\psi_5' = -\bar{U}_5\frac{\partial}{\partial x}\nabla^2\psi_5' - \frac{\partial\psi_5'}{\partial x}(\beta - \bar{U}_{5yy}) + \frac{f_0}{\rho_5\Delta Z_5}(-W_4') \tag{2.3}$$

$$\frac{\partial S_1'}{\partial t} = [(M_2' - W_2')(\bar{S}_2 - \bar{S}_1)]/\rho_1\Delta Z_1 - \bar{U}_1\frac{\partial S_1'}{\partial x} - \frac{\partial\psi_1'}{\partial x}\frac{\partial\bar{S}_1}{\partial y} \tag{2.4}$$

$$\frac{\partial S_3'}{\partial t} = [(M_2' - W_2')(\bar{S}_3 - \bar{S}_2) + (M_4' - W_4')(\bar{S}_4 - \bar{S}_3) - D_3 l_3 L]/\rho_3\Delta Z_3 - \bar{U}_3\frac{\partial S_3'}{\partial x} - \frac{\partial\psi_3'}{\partial x}\frac{\partial\bar{S}_3}{\partial y} \tag{2.5}$$

$$\frac{\partial S_5'}{\partial t} = [(M_4' - W_4')(\bar{S}_5 - \bar{S}_4) - D_5 l_5 L]/\rho_5\Delta Z_5 - \bar{U}_5\frac{\partial S_5'}{\partial x} - \frac{\partial\psi_5'}{\partial x}\frac{\partial\bar{S}_5}{\partial y} \tag{2.6}$$

$$\frac{\partial h_1'}{\partial t} = (M_2' - W_2')(\bar{h}_2 - \bar{h}_1)/\rho_1\Delta Z_1 - \bar{U}_1\frac{\partial h_1'}{\partial x} - \frac{\partial\psi_1'}{\partial x}\frac{\partial\bar{h}_1}{\partial y} \tag{2.7}$$

$$\frac{\partial h_3'}{\partial t} = [(M_2' - W_2')(\bar{h}_3 - \bar{h}_2) + (M_4' - W_4')(\bar{h}_4 - \bar{h}_3) + D_3(\bar{h}_3^* - \bar{h}_3)]/\rho_3\Delta Z_3 - \bar{U}_3\frac{\partial h_3'}{\partial x} - \frac{\partial\psi_3'}{\partial x}\frac{\partial\bar{h}_3}{\partial y} \tag{2.8}$$

$$\frac{\partial h_5'}{\partial t} = [(M_4' - W_4')(\bar{h}_5 - \bar{h}_4) + D_5(\bar{h}_5^* - \bar{h}_5)]/\rho_5\Delta Z_5 - \bar{U}_5\frac{\partial h_5'}{\partial x} - \frac{\partial\psi_5'}{\partial x}\frac{\partial\bar{h}_5}{\partial y}. \tag{2.9}$$

In these equations $S=(c_p\bar{T}+gZ)$ is the dry static energy, $h=(s+Lq)$ is the moist static energy, $\bar{U}$ the zonal wind, $\psi=(p/\rho f_0)$ the stream-function, M_c the total mass flux in the clouds, D the total detrainment, l the detrained liquid water and L the latent heat of condensation. Overbars denote the mean value, primes the perturbation value and asterisks the saturation value. The variables u, v, w, p, ρ, T, q are zonal velocity, meridional velocity, vertical velocity, pressure, density, temperature and mixing ratio, respectively; and $W=\rho w$, $v'=\partial\psi'/\partial x$ and $(\partial/\partial Z)(p'/\rho)=gs'/c_p\bar{T}$. Other symbols have their standard meaning.

The hydrostatic relation may be written

$$\psi_5'-\psi_3'=\alpha_5 S_5'+\alpha_3 S_3', \tag{2.10}$$

$$\psi_3'-\psi_1'=\alpha_3 S_3'+\alpha_1 S_1', \tag{2.11}$$

where

$$\alpha_j=\frac{g\Delta Z_j}{2c_p\bar{T}_j f_0}, \quad j=1, 3, 5.$$

Since $\bar{U}$ is a function of y and p, the equations are not separable and we have therefore followed the initial value approach.

At each time step the vertical velocity W is calculated by a diagnostic equation which is obtained by taking time derivatives of (2.10) and (2.11) and substituting in (2.1) through (2.6).

The perturbation ψ' is taken to be of the form

$$\psi'(x,y,p,t)=\mathrm{Re}\{\Psi(y,p,t)e^{ikx}\},$$

where Ψ is complex, i.e., $\Psi=\Psi_r+i\Psi_i$, and k is the wavenumber along x.

Phase speed C_r and growth rate $\nu=(kC_i)$ are calculated from the tendencies of Ψ, i.e.,

$$C_r=\frac{\Psi_i\dfrac{\partial\Psi_r}{\partial t}-\Psi_r\dfrac{\partial\Psi_i}{\partial t}}{k(\Psi_r^2+\Psi_i^2)},$$

$$\nu=kC_i=\frac{\Psi_r\dfrac{\partial\Psi_r}{\partial t}+\Psi_i\dfrac{\partial\Psi_i}{\partial t}}{\Psi_r^2+\Psi_i^2},$$

where $C=C_r+iC_i$ is the complex phase speed.

In this study, heating is considered a perturbation variable and is assumed to have a sinusoidal variation in the longitudinal direction. This is certainly a shortcoming of the study, because in observed synoptic waves precipitation is confined mainly to the convergent regions of the waves. This assumption has been made to simplify the mathematical analysis, because the specification of heating over only a certain portion of the wave and no specification of heating over the remaining portion of the wave makes the problem nonlinear, and would be difficult to incorporate in a linear stability analysis. Due to the assumption of sinusoidal heating, the horizontal scale of the region over which heating occurs is only half that of the wavelength of the perturbation. An equal amount of cooling takes place over the remaining half of the wavelength. The effect of this assumption, therefore, may be to enhance the rate of generation of available potential energy and thus to overestimate the magnitude of the growth rate. This model shortcoming may be partly corrected by introducing a mean heating term, which can compensate for the cooling effects of the sinusoidal heating perturbation. However, the incorporation of mean heating would involve the determination of the mean cloud mass flux. This aspect is beyond the scope of the present study.

Calculation of cloud mass flux by quasi-equilibrium assumption

The quasi-equilibrium assumption of Arakawa and Schubert (1974) has been used to calculate the cloud mass flux M_c. The cloud work function $A(\lambda)$ may be defined as

$$A(\lambda)=\int_{Z_B}^{Z_D}(g/c_p\bar{T})\eta(Z,\lambda)[S_c(Z,\lambda)-\bar{S}(Z,\lambda)]dZ, \tag{2.1.1}$$

where c refers to the cloud, and Z_B and Z_D are the base and the detrainment level for the cloud. A cloud type is identified by its fractional rate of entrainment λ such that

$$\lambda=\eta^{-1}\partial\eta/\partial Z. \tag{2.1.2}$$

The mass flux at height Z, $m(Z,\lambda)$ for cloud type λ, is given as $m(Z,\lambda)=m_B(\lambda)\eta(Z,\lambda)$, where $m_B(\lambda)$ is the mass flux at the base of the cloud type λ. The cloud mass flux

$$M_c(Z)=\int m(Z,\lambda)d\lambda$$

is calculated by solving an integral equation which is obtained by the quasi-equilibrium assumption (QEA), i.e.,

$$\frac{dA}{dt}=0. \tag{2.1.3}$$

The expressions for tendency of static energy are substituted from (2.4)–(2.9). For a detailed derivation of the continuous case see Arakawa and Schubert (1974) and for the discrete case, see Shukla (1976). It is assumed that the clouds entrain by their whole depth and detrain only at the level of vanishing buoyancy. In a three-layer model, only two kinds of clouds can be considered (see Fig. 3). The deep clouds which are fully precipitating detrain at level Z_5 and the nonprecipitating shallow clouds detrain at level Z_3. The height of the cloud base $Z_B=(Z_2)$ is assumed to be

constant with time. A model with time-dependent cloud base would require an adequate parameterization of the mixed layer and the subcloud layers.

Since the level of detrainment of the clouds is fixed and since S and h are being perturbed, it is necessary that the cloud ensemble readjusts its characteristic size to be consistent with its detrainment level. This is a consequence of the discreteness of the model. The expressions for the cloud mass flux M_2, M_4 and detrainment D_3 are derived in the Appendix.

In the earlier study by Shukla (1976), two kinds of clouds—the nonprecipitating, liquid water-detraining shallow clouds and the fully precipitating deep clouds—were included to parameterize the cumulus heating by QEA. Instability analysis of a resting atmosphere showed that the growth rate versus wavelength curve remained essentially the same for two cloud types as for deep clouds only. The effect of the shallow clouds, which detrain moisture and liquid water in the lower layer, is only to change the structure of the eigenfunctions. For the calculations in the present study, only the deep cloud model is used. For completeness, however, derivations are given for shallow and deep clouds both. It may be remarked that although such assumptions may not have serious effects on the results of a linear instability analysis where the mean state is assumed to be quasi-steady, absence of shallow clouds would adversely affect a numerical simulation where the main objective is to simulate the mean state. It should be noted, however, that in the case of one cloud model, the vertical profile of heating is determined by the entrainment parameter λ, and not by the structure of the wave fields. Therefore, for a given vertical structure of the mean moist static energy, the shape of the heating profile is fixed. However, the magnitude of the total cloud mass flux at the cloud base is determined by the application of quasi-equilibrium assumption.

3. Numerical integration of the model

The vertical structure of the model is shown in Fig. 3. No inflow or outflow is allowed through the vertical walls at 5°N and 28.75°N. The cloud base is assumed to be at 450 m which corresponds to the lifting condensation level at about 950 mb. The deep clouds, which detrain at 10.05 km, are assumed to be fully precipitating. This assumption may be justified from a study of Ramanamurty *et al.* (1960) whose observations suggest that during the monsoon season, most of the precipitation comes from the deep clouds.

The stepwise procedure for making the numerical integrations may be briefly stated as follows:

1) Calculate the values of the constant coefficients, which are determined by $\bar{S}$, $\bar{Z}$, $\bar{h}$, $\bar{U}$, appearing in the Appendix, for the mean monsoon atmosphere.

2) Assign the value of wavenumber k and assume an arbitrary perturbation, i.e.,

$$\psi(y,Z)=1.$$

3) Solve the diagnostic vertical velocity equation to obtain W_2 and W_4.

4) Obtain the values of M_2, M_4 and D_5 from the expressions given in the Appendix.

5) Integrate Eqs. (2.1)–(2.9). The numerical scheme for integrating these equations was exactly the same as described in Shukla (1977). The boundary conditions on the vertical velocity were (see Fig. 3)

$$W_0=W_E,$$
$$M_0=M_6=W_6=0.$$

6) Repeat the steps 3–5 for 100 time steps.

7) Calculate the values of growth rate and phase speed at each grid point of the domain and check for the convergence to a constant value. If they have converged to their constant value, further integration is discontinued. If not, go back to step 3 and continue the integration until convergence is reached.

8) Repeat the steps 2 through 7 for a range of values of the wavenumber k, and obtain a growth rate versus wavenumber curve and a phase speed versus wavenumber curve.

MAXIMUM GROWTH RATE AND MAXIMUM POTENTIAL FOR DOMINANCE

In interpreting the results of linear instability analysis, it is generally assumed that the wave having maximum growth rate would eventually dominate over the rest of the growing waves. The synoptic waves appearing on the weather charts are recognized as the possible manifestations of the fastest growing mode of the instability analysis.

In the case of barotropic or baroclinic instability, it may be reasonable to assume that the perturbations having the maximum growth rate will eventually dominate because they would "consume" most of the available kinetic or available potential energy. It is not clear if this would be so in the case of instabilities driven by moist convection because in this case, the extent to which a perturbation of a given wavelength may grow would be determined by the availability of moisture on the scale of that perturbation. Although the growth rate of the small-scale waves may be large, if the period of such waves is small, the total moisture evaporated over one period of the wave may not be sufficient to sustain the precipitation and therefore the maximum growth of the wave may not take place.

The actual equilibration mechanism for the tropical waves, which are driven primarily by cumulus heating, is not quite clear. Because of the nonlinearity connected with real condensational heating, an arbitrary flow may not be expressed as a superposition of linear eigenmodes, and it may not be possible, therefore, to apply a selection principle based on these considerations; i.e., the mode with the greatest growth rate does not necessarily dominate. We do not fully understand the roles of the mean motion and the availability of moisture in deter-

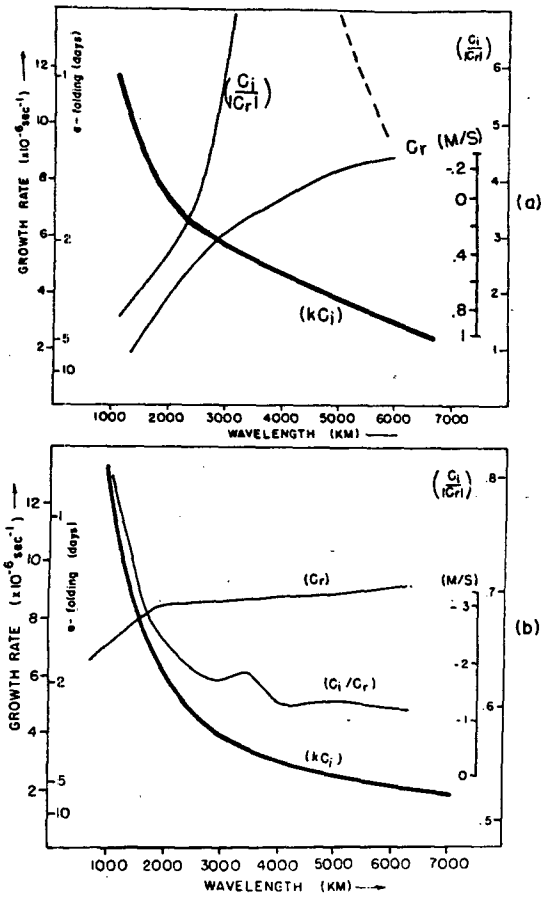

FIG. 4. Growth rate (kC_i), phase speed (C_r) and ratio (C_i/C_r) for the observed monsoon zonal wind $\bar{U}(y,z)$: (a) with Ekman pumping, (b) without Ekman pumping.

mining either the maximum possible amplitude of the tropical waves or the selection mechanism due to which the synoptic waves appear on the weather charts. Hayashi (1971) has hypothesized that the heating decreases with the increasing frequency of the waves so that the high frequency waves are stabilized. Lindzen (1974) has suggested that the equilibration of tropical waves may be determined by the way the waves modify the environment. The cumulus heating may modify the basic state in such a way that the most unstable modes may become neutral with respect to the modified environment. Kuo (1975) has suggested that the heating function should be scaled by the ratio of the period of the wave and a fixed period of eight days. This has the effect of reducing the heating and therefore the growth of the high-frequency waves.

In order to explain the appearance of synoptic-scale waves on the daily weather charts (even if the linear instability analysis may give the maximum growth rate for the smallest scale), we hypothesize that only those waves would "dominate" for which the ratio of their period to their e-folding time is maximum. Since the upper limit on the amplitude of a wave may be determined by its ability to utilize the available moisture, a wave may not dominate just because it has large growth rate. A large growth rate would only imply that it would equilibrate faster than other waves. The waves having larger periods may have the potential to dominate among all the growing waves.

In order to define the "potential for dominance", a quantity p is calculated as the ratio of the imaginary and the real parts of the complex phase speed. ($p=C_i/C_r$). The values of p are calculated for a range of wavelengths and, according to our hypothesis, the perturbation of that wavelength would have maximum potential for dominance for which p is maximum.

It should be emphasized that the above criteria, based on the ratio C_i/C_r to determine the most dominant perturbation, is only a hypothesis. This criteria breaks down for $C_r=0$. It is possible that for certain structures of the mean state, none of the criteria mentioned above suggest a dominant mode. In such a situation, we propose to examine the structure of those perturbations whose wavelength corresponds to that of the observed synoptic disturbances. A more rigorous criteria to explain the scale of the observed tropical waves awaits a clearer understanding of the equilibration mechanism for the tropical waves and their interaction with the mean motion. It may be interesting to note that for the case of resting atmosphere, the criteria based on the maxima of growth rate kc_i and the maxima of p yield the same value for the horizontal wavelength of the most unstable mode.

Fig. 4 shows the plots of growth rate kC_i, phase speed C_r and the ratio C_i/C_r for a range of wavelengths. Maximum values of growth rates are found for the smallest values of the horizontal wavelengths. The criteria based on the ratio C_i/C_r suggests that the perturbation with the wavelength of 3000 km may be the most dominant perturbation. The maximum values of C_i/C_r for the 3000 km perturbation occurs due to very small value of its phase speed. In this case, the application of the criteria based on the ratio C_i/C_r may be questionable.

For the case of Ekman pumping=0, plots of kC_i, C_r and C_i/C_r are shown in Fig. 4b. In this case, the growth rate kC_i and the ratio C_i/C_r are maximum for the smallest scale. Comparison of Figs. 4a and 4b suggests that the reduction in the phase speeds of the perturbations may be due to the addition of the Ekman pumping at the lowest boundary. It may be recalled that, in the case of the resting atmosphere, surface friction is essential for the existence of growing modes. For vertically shearing flow, the structure of the divergence field depends on the phase relationships among the internal vertical velocities generated by 1) the differential vorticity advection and thermal advection, 2) surface friction, and 3) cumulus heating. Since the structure of these vertical velocity fields is wavelength-dependent, the magnitudes of the growth rate and the phase speed depend on the structure of the mean state (i.e., $\bar{U}$,

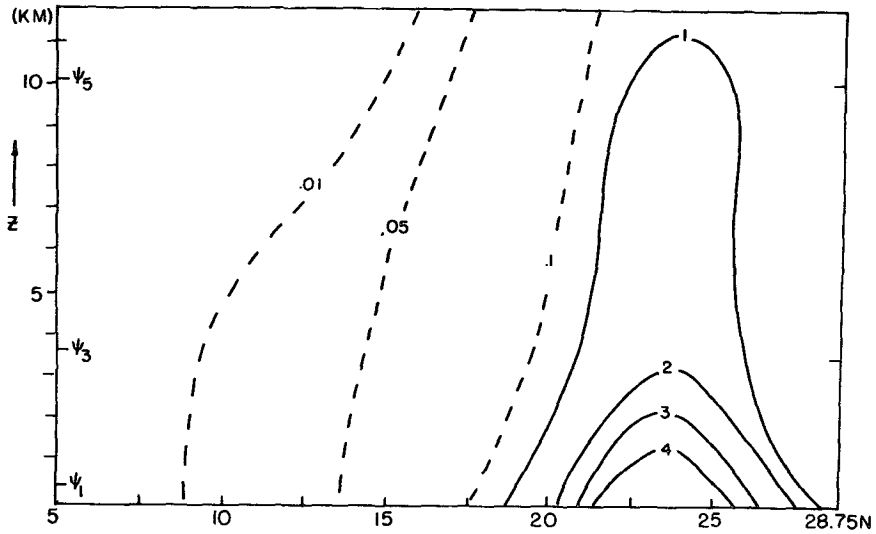

FIG. 5. Latitude-height cross section of the amplitude of (ψ) for the perturbation of wavelength 2500 km.

$\partial\bar{U}/\partial Z$, $\partial\bar{h}/\partial Z$), and the wavelength of the perturbation. Due to the complexity of the QEA parameterization, it has not been possible to isolate the effects of each factor in analytical form; therefore, we have presented the results of numerical integrations of linearized perturbation equations.

Since the wavelength of the monsoon depressions is in the range 2000–3000 km, we have made a detailed analysis of the structure and energetics of the computed perturbations for wavelengths of 2000, 2500 and 3000 km. The structure and energetics for the perturbations of these wavelengths were found to be nearly the same. For the case of zero Ekman pumping we have presented, in the following section, the structure and energetics for the 2500 km perturbation.

4. Structure of the computed perturbation

Fig. 5 shows the latitude-height cross section of the amplitude of ψ. The perturbation has appreciable vertical structure up to 10 km. The amplitude maximum is close to the observed location of the monsoon depressions. The vertical amplitude structure is also in agreement with the observations of Krishnamurti *et al.* (1975). The westward phase speed of the computed perturbations is comparable to the observed phase speed of the monsoon depressions.

In order to understand the possible mechanisms which produce maximum amplitude between 20 and 25°N, we carried out the barotropic instability analysis of the zonal wind at each level. It was found that for the case of $\partial\bar{U}/\partial Z=0$ and $\bar{U}(y)$ at each level equal to $\bar{U}(y)$ at Z_3 (3.64 km), the maximum amplitude occurred between 20 and 25°N. The results of a combined CISK-barotropic instability analysis of the zonal wind at Z_3 also showed that the amplitude was a maximum between 20°N and 25°N. It may therefore be suggested that the occurrence of maximum amplitude between 20°N and 25°N may be primarily due to the barotropic instability of the flow at 3.64 km. However, for the barotropic case and the CISK-barotropic case, the amplitude, at a given latitude, was a maximum at the highest level Z_5. The amplitude structure shown in

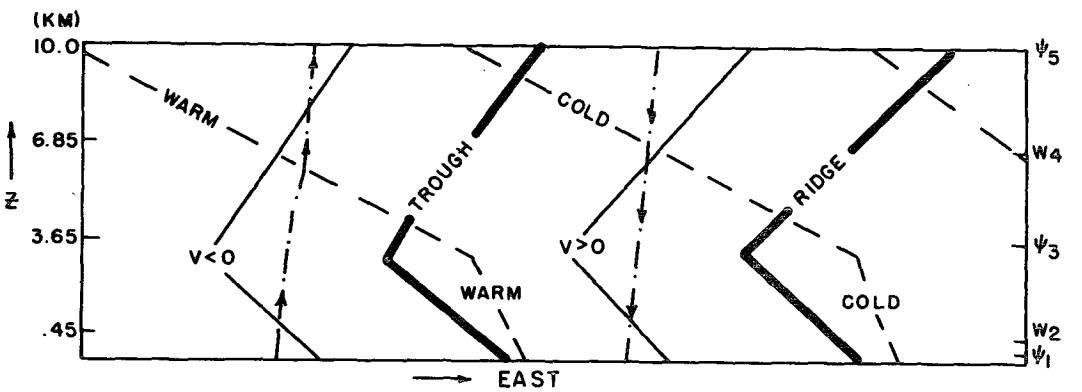

FIG. 6. Longitude-height cross section for the perturbation of wavelength 2500 km.

Fig. 5, which is similar to the structure of the observed monsoon depressions, occurred only when we considered the combined CISK-barotropic-baroclinic instability.

Fig. 6 shows the longitude-height cross section of the structure of the perturbation of wavelength 2500 km. The maxima of vertical velocity is found to be ahead (west) of the trough. This agrees with the conclusions of Krishnamurti *et al.* (1975). The trough and the ridge lines slope toward the east in the vertical, which is also in agreement with the observed slope of the monsoon depressions. Krishnamurti *et al.* (1975) have shown that the monsoon depression has a cold core in the lower layers and a warm core in the upper layers. The computed perturbations do not have such thermal structure. Warm advection takes place ahead (west) of the trough and the rising motions occur in the warmer sector of the wave. We believe that the observed low-level cold core may be due to the cooling caused by the evaporation of the falling rain. We have not included this effect in our model.

It should be further remarked that if cumulus heating were parameterized by QEA, in the presence of vertical shear only, the maximum growth rate would occur for the smallest scale. However, if $\partial\bar{U}/\partial Z=0$ and heating were parameterized by QEA, for the horizontally shearing flow at Z_3 the maximum growth rate would occur for a wavelength of intermediate scale ($\sim$2000 km).

5. Energetics of the computed perturbation

For the three-layer model described in Section 2, the energy equations may be given as

$$\frac{\partial K'}{\partial t}=C(KZ,KE)+C(AE,KE)-\epsilon',$$

$$\frac{\partial P'}{\partial t}=C(AZ,AE)-C(AE,KE)+C(QE,AE),$$

where K' is the eddy kinetic energy, P' the eddy potential energy, ϵ' the dissipation of eddy kinetic energy and $C(QE,AE)$ the conversion from heating to the eddy available potential energy. Other symbols are the same as defined in Section 2; r and i are subscripts for real and imaginary values. These terms are defined as follows:

$$K'=\frac{1}{2D}\int\left[\left\{k^2(\Psi_{rj}^2+\Psi_{ij}^2)+\left(\frac{\partial\Psi_{rj}}{\partial y}\right)^2+\left(\frac{\partial\Psi_{ij}}{\partial y}\right)^2\right\}\rho_j dZ_j\right]_{j=1,3,5}dy$$

$$P'=\frac{f_0}{2D}\int\left[\{\alpha_j(\bar{S}_{j+1}-\bar{S}_j)^{-1}(S_{rj}^2+S_{ij}^2)\}\rho_j dZ_j\right]_{j=1,3,5}dy$$

$$C(KE,KZ)=\frac{k}{2D}\int\left\{\frac{\partial\bar{U}_j}{\partial y}\left(\Psi_{ij}\frac{\partial\Psi_{rj}}{\partial y}-\Psi_{rj}\frac{\partial\Psi_{ij}}{\partial y}\right)\rho_j dZ_j\right\}_{j=1,3,5}dy$$

$$C(AZ,AE)=\frac{f_0 k}{2D}\int\left[\left\{\alpha_j\frac{\partial\bar{S}_j}{\partial y}(\bar{S}_j-\bar{S}_{j+1})^{-1}(\Psi_{rj}S_{ij}-\Psi_{ij}S_{rj})\right\}\rho_j dZ_j\right]_{j=1,3,5}dy$$

$$\epsilon'=\frac{f_0\epsilon_p}{2D}\int\left\{k^2(\Psi_{r1}^2+\Psi_{i1}^2)+\left(\frac{\partial\Psi_{r1}}{\partial y}\right)^2+\left(\frac{\partial\Psi_{i1}}{\partial y}\right)^2\right\}dy,\quad \epsilon_p=\tfrac{1}{2}\rho_0(2\nu/f_0)^{\frac{1}{2}},\quad \nu=100\ \mathrm{m^2\ s^{-1}}$$

$$C(AE,KE)=\frac{f_0}{2D}\int\left\{\begin{matrix}W_{r2}(\alpha_1S_{r1}+\alpha_3S_{r3})+W_{i2}(\alpha_1S_{i1}+\alpha_3S_{i3})\\+W_{r4}(\alpha_3S_{r3}+\alpha_5S_{r5})+W_{i4}(\alpha_3S_{i3}+\alpha_5S_{i5})\end{matrix}\right\}dy$$

$$C(QE,AE)=\frac{f_0}{2D}\int\left\{\begin{matrix}M_{r2}(\alpha_1S_{r1}+\alpha_3S_{r3})+M_{i2}(\alpha_1S_{i1}+\alpha_3S_{i3})\\+M_{r4}(\alpha_3S_{r3}+\alpha_5S_{r5})+M_{i4}(\alpha_3S_{i3}+\alpha_5S_{i5})\end{matrix}\right\}dy.$$

(D is the width of the domain.)

Fig. 7a shows the energy diagram for the computed perturbation of 2500 km wavelength and Fig. 7b the energy diagram presented by Krishnamurti *et al.* (1976). These authors have stated that the presently available network was found to be inadequate for the computation of the energy transformations from the observations of a single case study. The energy diagram of Fig. 7b was prepared from the data generated by numerical weather prediction from a multi-level primitive equation model. The primary difference between the energetics of the computed linear perturbations and the energetics based on the results of integration of multi-level model is found in the baroclinic conversions. The computed perturbations are found to be baroclinically damped, whereas the energy diagram given by Krishnamurti *et al.* shows that the zonal available potential energy is transformed to the eddy available

potential energy. The energy transformations from eddy available potential energy to eddy kinetic energy and from zonal kinetic energy to eddy kinetic are nearly the same in Figs. 7a and 7b. The largest conversions occur from eddy available potential energy to eddy kinetic energy. The dominant energy source for the generation of the dddy available potential energy is the condensational heating. The conversion from zonal kinetic energy to eddy kinetic energy is relatively small in both the cases. This diagram highlights the important role of moist-convective heating for the energetics of the monsoon depressions.

6. Summary and conclusion

A three-layer quasi-geostrophic model was used to investigate the instability of the horizontally and vertically shearing mean monsoon flow. The quasi-equilibrium assumption of Arakawa and Schubert was used to parameterize the effects of moist convection. One of the striking features of the calculations was the occurrence of maximum growth rate for the smallest scale.

The occurrence of maximum growth rate for the smallest scale may be either due to inadequate treatment of the subcloud layer or to the parameterization of cumulus heating by the quasi-equilibrium assumption. In reality, for cumulus convection to take place, the boundary layer convergence must be sufficient to lift the low-level air up to the lifting condensation level. The scale of the vertical circulations, associated with small horizontal scales, is also very small. The small-scale perturbations may not provide the necessary lifting needed to set in the cumulus convection. Therefore, all the perturbations with the horizontal scale smaller than the Rossby radius of deformation, corresponding to the vertical scale of the height of the lifting condensation level, should be stable. In the present model, the treatment of the subcloud layer is very simple. The vertical resolution is not adequate to identify the top of the mixed layer and the lifting condensation level. A more realistic treatment of the mixed layer, including the time variations of the depth of the mixed layer and the height of the cloud base, is beyond the scope of this study. A time-dependent mixed layer may introduce a constraint on the intensity of convection.

In the presence of vertical shear the cloud mass flux is found to be inversely proportional to the wavelength of the perturbation. Since heating is proportional to M_C in the QEA parameterization and the vertical velocity is determined by heating and large-scale vorticity and temperature advections, the vertical velocity, and therefore the heating, is found to be maximum for the smallest scale. This was confirmed by examining the eigenfunctions for the largest eigenvalues for a range of wavelengths in the case of vertical shear.

The structure and the energetics were studied for those perturbations which have horizontal scales in the range 2500–3500 km, which is a reasonable scale for monsoon depressions. The structure and the energetics of the computed perturbations and the observed monsoon depression were compared. In the absence of the Ekman pumping, the westward phase speeds of the computed perturbations were comparable to the actual phase speeds of observed monsoon depressions. However, when the effect of the Ekman pumping was added, the phase velocity was reduced. The amplitudes of the computed perturbations were a maximum between 20 and 25°N, which is reasonably close to the observed location of the most cyclogenetic area in the Bay of Bengal. The model perturbations had significant amplitudes up to 10 km, and the amplitudes were maximum in the lowest layers. This is in reasonable agreement with the observed amplitude structure of the monsoon depressions. The computed perturbations were found to have a warm core, whereas the observed monsoon depressions are found to have a cold core in the lower layers, and a warm core in the upper layers. If the cold core exists it may be due to the cooling caused by the evaporation of the falling rain. This effect was not included in our model.

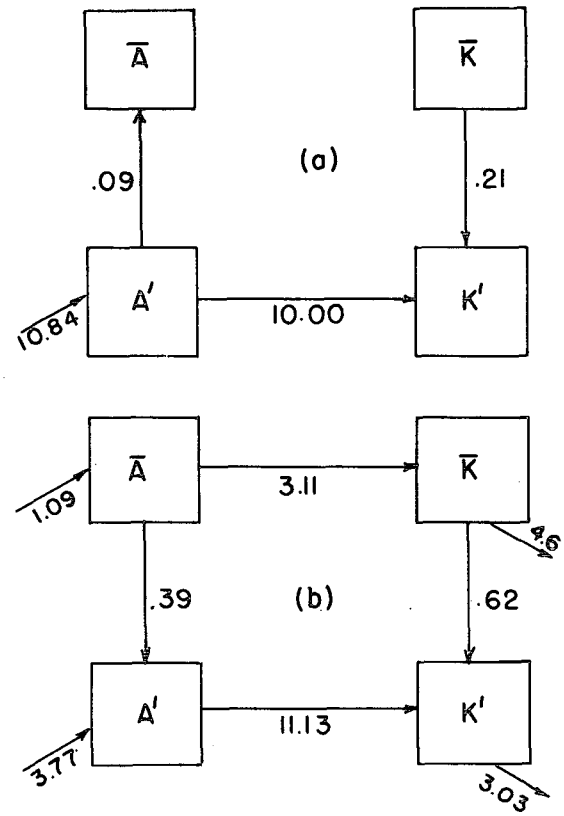

FIG. 7. Energy transformations for (a) computed perturbation of wavelength 2500 km and (b) results of Krishnamurti *et al.* (1976).

The dominant energy transformation for the computed perturbations was found to be from eddy available potential energy to eddy kinetic energy. The

primary source of energy is condensational heating. The transformation from zonal available potential energy to eddy available potential energy was small but negative, indicating that baroclinic instability is not important. For the computed perturbations, which are being driven primarily by cumulus heating, the barotropic conversion was found to be from zonal kinetic energy to eddy kinetic energy. Krishnamurti *et al.* (1976) also found that the major energy exchange is from eddy available potential energy to eddy kinetic energy and the conversion from zonal available potential energy to eddy available potential is relatively small. The barotropic energy exchange in their case also was from zonal kinetic energy to eddy kinetic energy. The results suggest that the magnitudes of the growth rates and the dominant energy transformations are determined by the CISK, the horizontal amplitude structure is determined by the horizontal shears, and the vertical amplitude structure is determined by the combined effects of vertical shear and condensational heating. These suggestions are made on the basis of the results of a linear perturbation model and further observational and theoretical studies will be needed to explain actual cyclogenesis over the Bay of Bengal. In particular, it may be desirable to investigate the moisture supply provided by the Bay of Bengal, as well as the details of the surrounding topography to arrive at an actual explanation.

From the results of the present study, it may be hypothesized that the primary role of the terrain is to produce a mean circulation (*viz.*, monsoon trough at the foothills of the Himalayas) which is barotropically unstable at the lower levels and which thus provides the "triggering" mechanism for the monsoon depressions. These, however, are amplified and maintained by latent heat of condensation.

Reasonable agreement in structure and energetics between the computed and the observed perturbations suggests that CISK is the primary driving mechanism for the growth of monsoon depressions.

Acknowledgments. The author expresses his gratitude to Prof. J. G. Charney for his encouragement, suggestions and stimulating discussions throughout the course of this study. The author is extremely grateful to Professor A. Arakawa for several valuable discussions on his scheme for cumulus parameterization. Several valuable conversations with John Roads regarding numerical integrations are gratefully acknowledged.

APPENDIX

Cloud Mass Flux, Detrainment and Vertical Motion in a Discrete Model

1. Calculation of cloud mass flux

If $m_B(s)$ and $m_B(d)$ denote the mass flux at the base of the shallow and deep clouds, respectively, the expressions for the total mass flux at levels Z_2 and Z_4 and detrainment at levels Z_3 and Z_5 may be given as (see Fig. 3)

$$\left.\begin{aligned} M_2&=m_B(s)+m_B(d)\\ M_4&=\eta_{d,4}m_B(d)\\ D_3&=m_B(s)\eta_{s,3}\\ D_5&=m_B(d)\eta_{d,5}\end{aligned}\right\}, \tag{A1}$$

where subscripts s and d are used for shallow and deep clouds, respectively, and $\eta_{d,4}$ represents the value of η for the deep clouds at level Z_4. From Eq. (2.1.2),

$$\eta_{d,4}=\exp[\lambda_d(Z_4-Z_2)]\approx 1+\lambda_d(Z_4-Z_2).$$

The procedure for calculating $m_B(s)$ and $m_B(d)$ consists of solving two equations

$$\left.\begin{aligned} \frac{dA(\lambda_s)}{dt}&=0\\ \frac{dA(\lambda_d)}{dt}&=0\end{aligned}\right\}. \tag{A2}$$

These two equations lead to two linear equations in $m_B(s)$ and $m_B(d)$, and their solution gives $m_B(s)$ and $m_B(d)$ as a function of ψ', S', h'. This was the purpose of parameterization.

For the three-layer model shown in Fig. 3, the following definitions apply:

$$A(d)=\frac{g}{c_p\bar{T}_3(1+\gamma_3)}[\eta_{d,4}h_{d,4}+\eta_{d,2}h_{d,2}-h_3^*(\eta_{d,4}+\eta_{d,2})]\Delta Z_3/2+\frac{g}{c_p\bar{T}_5(1+\gamma_5)}[\eta_{d,4}h_{d,4}-h_5^*\eta_{d,4}]\Delta Z_5/2,$$

where

$$\gamma_j=\frac{L}{c_p}\left(\frac{\partial q^*}{\partial T}\right)_{pj},\quad j=3,5,$$

$$S_c-S=(h_c-h^*)/(1+\gamma),$$

$$A(s)=\frac{g}{c_pT_3(1+\gamma_3)}(h_1-h_3^*)\Delta Z_3/2,$$

$$h_{d,5}=\frac{1}{\eta_{d,5}}[h_{d,2}+(\eta_{d,4}-\eta_{d,2})h_3+(\eta_{d,5}-\eta_{d,4})h_5],$$

$$h_{d,4}=\frac{1}{\eta_{d,4}}[h_{d,2}+(\eta_{d,4}-\eta_{d,2})h_3],$$

$$h_{s,3}=\frac{1}{\eta_{s,3}}[h_{s,2}+(\eta_{s,3}-\eta_{s,2})h_3],$$

$$\eta_{s,3}=1+\lambda_S(Z_3-Z_2),$$

$$\eta_{d,j}=1+\lambda_d(Z_j-Z_2),\quad j=2,3,4,5,$$

where

$$h_{C,2}=h_{d,2}=h_1, \qquad \lambda_d=\frac{h_1-h_5^*}{[h_5^*(Z_5-Z_2)-h_3(Z_4-Z_2)-h_5(Z_5-Z_4)]}, \qquad \lambda_s=\frac{h_1-h_3^*}{(h_3^*-h_3)(Z_3-Z_2)}.$$

Eqs. (A2) yield the following two linear equations in $m_B(s)$ and $m_B(d)$:

$$\{[m_B(s)+m_B(d)]-W_2'\}\left(\frac{\bar{h}_2-\bar{h}_1}{\rho_1\Delta Z_1}\right)-\bar{U}_1\frac{\partial h_1'}{\partial x}-\frac{\partial \bar{h}_1}{\partial y}\frac{\partial \psi_1'}{\partial x}$$

$$-(1+\gamma_3)\Big[\{[(M_B(s)+m_B(d))-W_2'](\bar{S}_3-\bar{S}_2)+[\eta_{d,4}m_B(d)-W_4'](\bar{S}_4-\bar{S}_3)-D_3Ll_{s,3}\}/\rho_3\Delta Z_3$$

$$+\left(-\bar{U}_3\frac{\partial S_3'}{\partial x}-\frac{\partial \bar{S}_3}{\partial y}\frac{\partial \psi_3'}{\partial x}\right)\Big]=0, \quad \text{(A3)}$$

$$f_1\Big[[\{m_B(s)+m_B(d)\}-W_2']\left(\frac{\bar{h}_2-\bar{h}_1}{\rho_1\Delta Z_1}\right)-\bar{U}_1\frac{\partial h_1'}{\partial x}-\frac{\partial \bar{h}_1}{\partial y}\frac{\partial \psi_1'}{\partial x}\Big]$$

$$+f_3\Big\{\{[(m_B(s)+m_B(d))-W_2'](\bar{S}_3-\bar{S}_2)+[\eta_{d,4}m_B(d)-W_4'](\bar{S}_4-\bar{S}_3)-D_3Ll_{s,3}\}/\rho_3\Delta Z_3$$

$$+\left(-\bar{U}_3\frac{\partial S_3'}{\partial x}-\frac{\partial \bar{S}_3}{\partial y}\frac{\partial \psi_3'}{\partial x}\right)\Big\}(1+\gamma_3)$$

$$+f_4\Big[\{[(m_B(d)\eta_{d,4}-W_4')](\bar{h}_5-\bar{h}_4)+D_5(\bar{h}_5^*-\bar{h}_5)]/\rho_5\Delta Z_5+\left(-\bar{U}_5\frac{\partial h_5'}{\partial x}-\frac{\partial \bar{h}_5}{\partial y}\frac{\partial \psi_5'}{\partial x}\right)\Big]$$

$$+f_2\Big[\{[(m_B(s)+m_B(d))-W_2'](\bar{h}_3-\bar{h}_2)+[\eta_{d,4}m_B(d)-W_4'](\bar{h}_4-\bar{h}_3)+D_3(\bar{h}_3^*-\bar{h}_3)\}/\rho_3\Delta Z_3$$

$$+\left(-\bar{U}_3\frac{\partial h_3'}{\partial x}-\frac{\partial \bar{h}_3}{\partial y}\frac{\partial \psi_3'}{\partial x}\right)\Big]+f_5(1+\gamma_5)\Big[\{m_B(d)\eta_{d,4}-W_4'\}\frac{(\bar{S}_5-\bar{S}_4)}{\rho_5\Delta Z_5}-\bar{U}_5\frac{\partial S_5'}{\partial x}-\frac{\partial \bar{S}_5}{\partial y}\frac{\partial \psi_5'}{\partial x}\Big]=0, \quad \text{(A4)}$$

where

$$f_1=R_1+R_3(1+R_6)/\eta_{d,4}+R_5R_7,$$

$$f_2=R_3(\eta_{d,4}-\eta_{d,2})(1+R_6)/\eta_{d,4}+R_5(\eta_{d,4}-\eta_{d,2})R_7,$$

$$f_3=R_2,$$

$$f_4=(\eta_{d,5}-\eta_{d,4})\{R_3R_6/\eta_{d,4}+R_5R_7\},$$

$$f_5=-\left\{\frac{\eta_{d,4}g}{c_pT_5(1+\gamma_5)}+\eta_{d,5}(R_3R_6/\eta_{d,4}+R_5R_7)\right\},$$

$$R_1=\frac{g\Delta Z_3}{c_pT_3(1+\gamma_3)\Delta Z_5}, \qquad R_2=-R_1(1+\eta_{d,4}),$$

$$R_3=\eta_{d,4}R_1-R_4, \qquad R_4=\frac{-g\eta_{d,4}}{c_pT_5(1+\gamma_5)},$$

$$R_5=\left[\frac{g\Delta Z_3}{c_pT_3(1+\gamma_3)\Delta Z_5}\{\bar{h}_{d,4}-\bar{h}_3^*\}+\frac{g}{c_pT_5(1+\gamma_5)}\{\bar{h}_{d,4}-\bar{h}_5^*\}\right]\frac{\partial\eta_{d,4}}{\partial\lambda_d},\quad R_6=R_7\left\{\frac{\partial\eta_{d,5}}{\partial\lambda_d}(\bar{h}_5^*-\bar{h}_5)+\frac{\partial\eta_{d,4}}{\partial\lambda_d}(\bar{h}_5-\bar{h}_3)\right\},$$

$$R_7=\frac{\partial\eta_{d,4}}{\partial\lambda_d}(\bar{h}_3-\bar{h}_{d,4}),$$

$$l_{s,3}=\left[\frac{\bar{q}_1+\lambda_s(Z_3-Z_2)\bar{q}_3}{\eta_{s,3}}-\bar{q}_3^*\right],$$

$$\frac{\partial\lambda_d}{\partial t}=\frac{\dfrac{\partial h_1'}{\partial t}+(\eta_{d,4}-\eta_{d,2})\dfrac{\partial h_3'}{\partial t}+(\eta_{d,5}-\eta_{d,4})\dfrac{\partial h_5'}{\partial t}-\eta_{d,5}\dfrac{\partial h_5^*}{\partial t}}{\dfrac{\partial\eta_{d,5}}{\partial\lambda_d}(\bar{h}_5^*-\bar{h}_5)+\dfrac{\partial\eta_{d,4}}{\partial\lambda_d}(\bar{h}_5-\bar{h}_3)}.$$

2. Diagnostic equation for W_2 and W_4

W_2 and W_4 are obtained by solving the two equations

$$\nabla^2\frac{\partial}{\partial t}(\psi_5'-\psi_3')=\nabla^2\frac{\partial}{\partial t}(\alpha_5S_5'+\alpha_3S_3'),$$

$$\nabla^2\frac{\partial}{\partial t}(\psi_3'-\psi_1')=\nabla^2\frac{\partial}{\partial t}(\alpha_3S_3'+\alpha_1S_1'),$$

where

$$\alpha_j=\frac{g\Delta Z_j}{2c_pT_jf_0},\quad j=1,3,5.$$

Time derivatives of ψ' and S' are substituted from (2.1) through (2.6).

REFERENCES

Arakawa, A., and W. H. Schubert, 1974: Interaction of a cumulus cloud ensemble with the large-scale environment. Part I. *J. Atmos. Sci.*, **31**, 674–701.

Charney, J. G., 1971: Tropical cyclogenesis and the formation of the ITCZ. *Lectures in Applied Mathematics*, Vol. 13, Amer. Math. Soc., 355–368.

——, 1973: Movable CISK. *J. Atmos. Sci.*, **30**, 50–52.

——, and M. E. Stern, 1962: On the stability of internal baroclinic jets in a rotating atmosphere. *J. Atmos. Sci.*, **19**, 159–172.

India Meteorological Department, 1971: Forecasting Manual. India Meteorological Department, Poona-5, India. [Available from Director General of Observatories, New Delhi, India.]

Hayashi, Y., 1971: Instability of large-scale equatorial waves with a frequency-dependent CISK parameter. *J. Meteor. Soc. Japan*, **49**, pp. 59–62.

Krishnamurti, T. N., M. Kanamitsu, R. Godbole, C. B. Chang, F. Carr and J. H. Chow, 1975: Study of a monsoon depression. (I) Synoptic structure. *J. Meteor. Soc. Japan*, **53**, 227–240.

——, ——, ——, ——, —— and ——, 1976: (II) Dynamic structure. *J. Meteor. Soc. Japan*, **54**, 208–225.

Kuo, H. K., 1975: Instability theory of large-scale disturbances in the tropics. *J. Atmos. Sci.*, **32**, 2229–2245.

Lindzen, R. S., 1974: Wave-CISK in the tropics. *J. Atmos. Sci.*, **31**, 156–179.

Ramage, C. S., and C. R. V. Raman, 1972: *International Indian Ocean Meteorological Atlas*, Vol. 2, *Upper Air*. [Available from National Science Foundation.]

Ramanna, G. R., 1967: Relationships between depressions of Bay of Bengal and tropical storms of the China sea. *Indian J. Meteor. Geophys.*, **18**, 148–150.

Ramanamurty, Bh. V., K. R. Biswas and B. K. G. Dastidar, 1960: Incidence of "warm" and "cold" rain in and around Delhi, and their contributions to season's rainfall. *Indian J. Meteor. Geophys.*, **11**, 331–346.

Saha, K. R., and S. S. Singh, 1972: On the distribution of mean static stability and mean Richardson number in tropical atmosphere. *J. Meteor. Soc. Japan*, **50**, 312–323.

Shukla, J., 1976: On the dynamics of monsoon disturbances. Sc.D. thesis, MIT, 178 pp.

——, 1977: Barotropic-baroclinic instability of mean zonal wind during summer monsoon. *Pure Appl. Geophys.*, **115**, 1449–1462.